Journal of the European Ceramic Society **19** (1999) 2909–2915

PII: S0955-2219(99)00076-X
0955-2219/99/$ - see front matter

Sintering and Decomposition of Ferroelectric Layered Perovskites: Strontium Bismuth Tantalate Ceramics

Chung-Hsin Lu* and Yi-Chou Chen

Department of Chemical Engineering, National Taiwan University, Taipei, Taiwan

(Received 17 September 1998; accepted 13 March 1999)

Abstract

The sintering behavior of layered-type perovskite ferroelectric ceramics $SrBi_2Ta_2O_9$ has been investigated in this study. Pure $SrBi_2Ta_2O_9$ powder is difficult to sinter at low temperatures. Raising the sintering temperature induces an increase in the density of $SrBi_2Ta_2O_9$, and also causes its thermal decomposition, thereby resulting in the formation of a secondary phase-$SrTa_2O_6$. On the other hand, adding excess amounts of Bi_2O_3 ($\geq$2 mol%) in $SrBi_2Ta_2O_9$ facilitates the densification process and suppresses the decomposition reaction. $SrBi_2Ta_2O_9$ ceramics with a density higher than 95% theoretical have been successfully prepared after sintering at 1100°C. The microstructure and crystallographic orientation are significantly influenced by the sintering temperature as well as the amount of Bi_2O_3 addition. Increasing the amount of Bi_2O_3 and sintering temperature enhances the development of the preferred orientation along the c*-axis and the coarsening of grains. The occurrence of the* c*-axis preferred orientation is ascribed to anisotropic grain growth.*

Keywords: decomposition, strontium bismuth tantalate, sintering, perovskites, tantalates.

1 Introduction

Recently ferroelectric materials are attracting interest for their application in ferroelectric random access memories (FRAM). These memories may replace the silicon-based electrically erasable programmable read-only memories (EEPROM) as they possess low operating voltage, high reading and writing speed, and nonvolatility.[1–5] $PbZr_xTi_{1-x}O_3$ (PZT) has been a promising material for the application of FRAM; however, it suffers severe polarization fatigue on platinum electrodes after long switching cycles. In order to improve the resistance to fatigue, conductive oxide electrodes have been used, but they have lower electrical conductivity than platinum electrodes.[4,5] On the other hand, $SrBi_2Ta_2O_9$ has been found to exhibit high fatigue resistance and polarization retention up to 10^{12} switch cycles on Pt electrodes.[6] This material also possesses low leakage current as well as low operating voltage. Because of these excellent electrical properties, $SrBi_2Ta_2O_9$ is an attractive material for FRAM.

$SrBi_2Ta_2O_9$ is a layered-type perovskite ferroelectric. This family was first synthesized and investigated by Aurivillius in 1949.[7] The general formula for Bi-containing layered-type compounds is $Bi_2O_2A_{n-1}B_nO_{3n+1}$. For $SrBi_2Ta_2O_9$, n is equal to 2, and A and B are Sr and Ta, respectively. The structure of $SrBi_2Ta_2O_9$ contains a stacking along the *c*-axis of two perovskite-like TaO_6 octahedron units between $(Bi_2O_2)^{2+}$ layers, whereas strontium cations are located in the space between TaO_6 octahedrons.[8] The crystal structure has orthorhombic symmetry with $a = 0{\cdot}5306$ nm, $b = 0{\cdot}55344$ nm, and $c = 2{\cdot}49839$ nm; the theoretical density is $8{\cdot}785\ g\,cm^{-3}$.[9]

$SrBi_2Ta_2O_9$ films have been successfully prepared by physical vapor deposition (PVD),[10–15] metal–organic decomposition (MOD),[16–18] metal-organic chemical vapor deposition (MOCVD),[19] and sol–gel processing.[20,21] The thin films prepared by all these techniques possess excellent ferroelectric characteristics and fatigue resistance. Different hypotheses have also been proposed for the anti-fatigue mechanism of $SrBi_2Ta_2O_9$ films.[22,23] Extensive studies have been carried out on thin films of $SrBi_2Ta_2O_9$, but less research on bulk ceramics of $SrBi_2Ta_2O_9$ has been performed. For PVD processes such as RF sputtering and laser deposition,

* To whom all correspondence should be addressed. Fax: +886-2362-3040.

preparation of densified $SrBi_2Ta_2O_9$ target ceramics is important. The bulk density, preferred orientation, and stoichiometry of the target will affect the deposition rate, phase content, and homogeneity of the thin films obtained.[24,25] Hence, an understanding of the sintering behavior of $SrBi_2Ta_2O_9$ ceramics is important.

In this study, the sintering behavior of pure $SrBi_2Ta_2O_9$ powder is investigated first. For improved densification, excess amounts of Bi_2O_3 are added. Optimal sintering conditions for obtaining densified and non-decomposed ceramics are determined. In addition, the variation in the crystallographic orientation and the microstructure after sintering are investigated.

2 Experimental Procedure

$SrBi_2Ta_2O_9$ powder was prepared via a two-stage process using $BiTaO_4$ as precursor.[26,27] Bi_2O_3 and Ta_2O_5 were ball-milled in equal molar ratio with ethyl alcohol for 48 h using zirconia balls. The mixed slurry was then dried and calcined in an electrical furnace at a heating rate of $10^{\circ}C\,min^{-1}$ and quenched at 900°C to obtain pure $BiTaO_4$. The obtained $BiTaO_4$ powder was subsequently mixed with $SrCO_3$ in stoichiometric ratio, followed by similar ball-milling and drying processes. After the mixed powder was heated and quenched at 900°C, pure $SrBi_2Ta_2O_9$ powder was obtained. The particle size was around 0·1–0·2 μm. For better sinterability, various amounts of Bi_2O_3 were added. We denote powders doped with 1, 2, and 4 mol% excess Bi_2O_3 as SBT1, SBT2, and SBT4, respectively, and the non-doped powder as SBT.

The prepared powders were uniaxially pressed at 98 MPa into pellets of 8 mm in diameter. These pellets were sintered at temperature ranging from 1000 to 1300°C for 1–2 h. After sintering, the densities of the sintered pellets were measured, and the phase and crystallographic structure were identified by X-ray powder diffraction (XRD) analysis using CuK_α radiation. The microstructural evolution during sintering was investigated by scanning electron microscopy (SEM). The compositional analysis was carried out via energy dispersive X-ray spectroscopy (EDS).

3 Results and Discussion

3.1 Sintering behavior of $SrBi_2Ta_2O_9$

The sintering behavior of the pressed specimens is illustrated in Fig. 1. At 1000°C the density of pellets remains nearly that of the as-pressed pellets. The densities for pellets sintered at 1250°C for 1 and 2 h reach maximum values of 8·30 and 8·38 $g\,cm^{-3}$, respectively. The surfaces of sintered specimens were examined by XRD (shown in Fig. 2). After 1100°C-sintering a well-developed crystal structure of $SrBi_2Ta_2O_9$ is identified, and no secondary phase is observed. However, at temperature higher than 1150°C, a secondary phase-$SrTa_2O_6$ with a tungsten bronze structure is found.[28] At temperatures higher than 1250°C, all $SrBi_2Ta_2O_9$ disappears and only $SrTa_2O_6$ is observed on the pellet surface. The observed decomposition of $SrBi_2Ta_2O_9$ is considered to proceed as below:

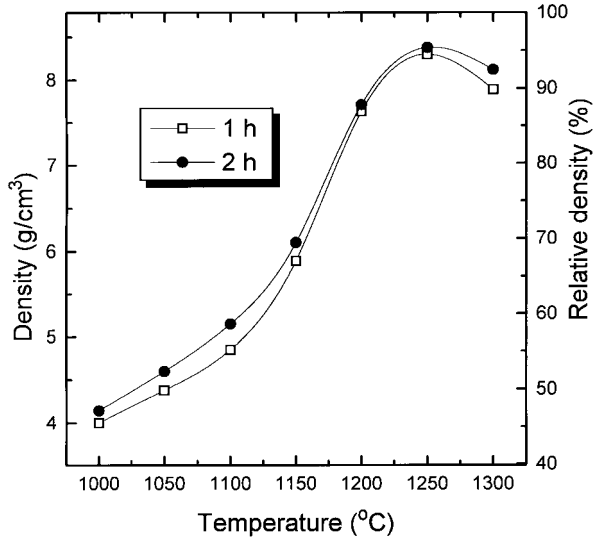

Fig. 1. Density of $SrBi_2Ta_2O_9$ as a function of sintering temperature.

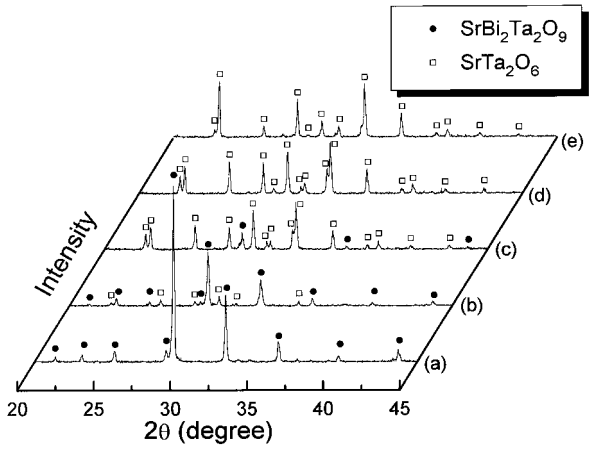

Fig. 2. X-ray diffraction patterns of the specimen surface of $SrBi_2Ta_2O_9$ sintered at (a) 1100°C, (b) 1150°C, (c) 1200°C, (d) 1250°C, and (e) 1300°C for 1 h.

$$SrBi_2Ta_2O_9 \rightarrow SrTa_2O_6 + Bi_2O_3 \quad (1)$$

Since Bi_2O_3 is highly volatile, it is easily vaporized from the specimen surface at elevated temperatures. Therefore, no Bi_2O_3 is detected by XRD. From the above sintering experiments and XRD results, it is found that $SrBi_2Ta_2O_9$ is hardly sintered at low temperatures. Raising the heating temperature can

increase the density of specimens, but it also induces the decomposition of $SrBi_2Ta_2O_9$. Accordingly, in order to maintain the original structure of $SrBi_2Ta_2O_9$, the highest available sintering temperature should be 1100°C. However, at this temperature the relative density of specimens is only 58·6% of the theoretical value for 2 h-sintering.

3.2 Effect of the addition of excess Bi_2O_3 on sintering and thermal stability of $SrBi_2Ta_2O_9$

In order to improve densification of $SrBi_2Ta_2O_9$ and suppress its decomposition, various amounts of Bi_2O_3 were added. Figure 3 shows the influence of the addition of Bi_2O_3 on the sintering behavior of $SrBi_2Ta_2O_9$. With 1 mol% Bi_2O_3 (SBT1), the density of these specimens reaches a maximum value at 1200°C of 8·32 g cm^{-3} (94·7%). 2 and 4 mol% (SBT2 and SBT4) Bi_2O_3 have distinct effects on sintering. At 1100°C, the density of SBT2 increases to 8·46 g cm^{-3} (96·3%). While in the case of SBT4, the specimens are easily sintered even as low as 1000°C. At 1100°C, the density of pellets reaches a maximum value, 8·40 g cm^{-3} (95·6%). The densities tend to decrease at higher temperatures due to the decomposition of $SrBi_2Ta_2O_9$.

The percent linear change and differential coefficient of expansion curves for 4 mol% Bi_2O_3-doped (SBT4) and non-doped specimens (SBT) are illustrated in Figs 4(a) and (b), respectively. The shrinkage of SBT4 occurs rapidly between 800 and 1000°C. It is reported that the melting point of Bi_2O_3 is 824°C.[29] Therefore, it is considered that the rapid shrinkage of SBT4 above 800°C results from the formation of a liquid phase which promotes densification liquid-phase sintering. Similar effects of Bi_2O_3 on the sintering of ceramics have been reported for $Bi_4Ti_3O_{12}$ and ZnO.[30,31]

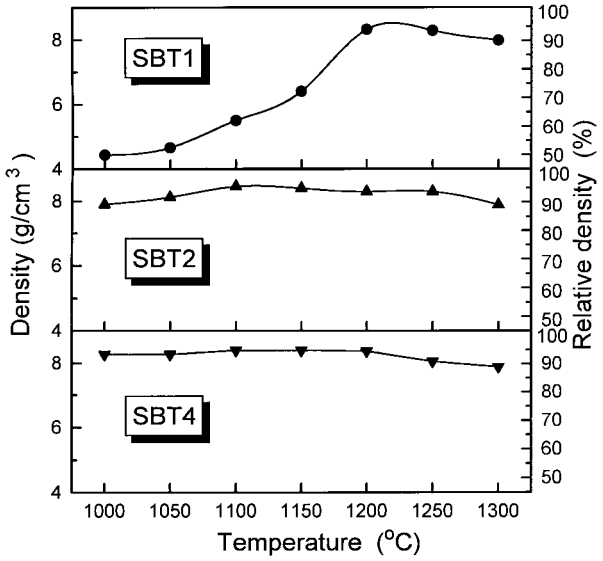

Fig. 3. Density of SBT1, SBT2, and SBT4 as a function of sintering temperature.

The surfaces of the doped specimens were examined by XRD. The results for specimens sintered at 1100 and 1150°C are presented in Figs 5 and 6, respectively. It is found that only $SrBi_2Ta_2O_9$ is

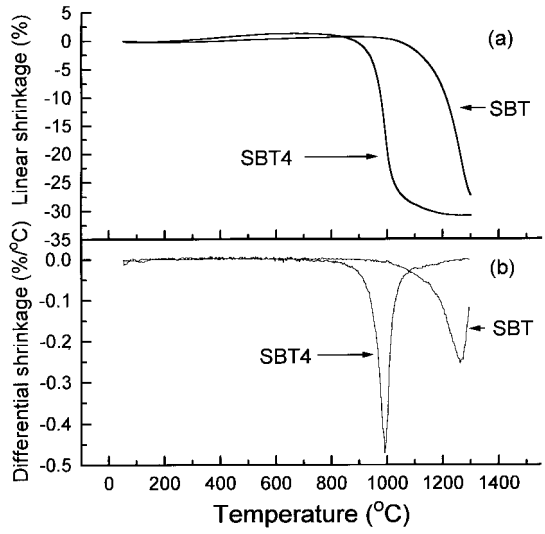

Fig. 4. (a) Percent linear change and (b) differential coefficient of expansion of $SrBi_2Ta_2O_9$ (SBT) and SBT4.

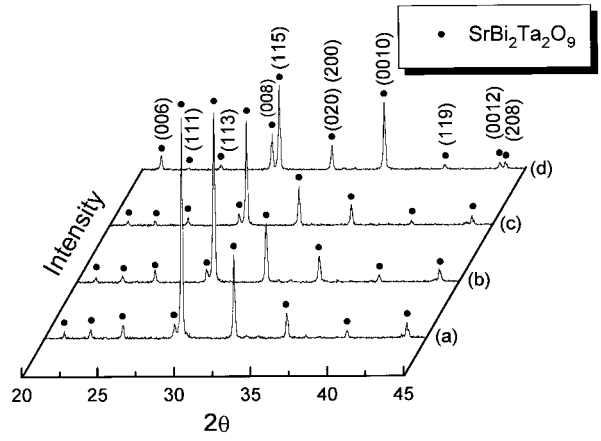

Fig. 5. X-ray diffraction patterns of the specimen surface of (a) SBT, (b) SBT1, (c) SBT2, and (d) SBT4 sintered at 1100°C.

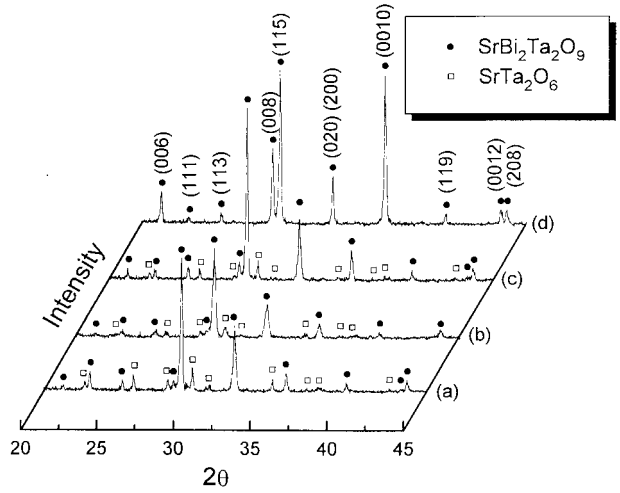

Fig. 6. X-ray diffraction patterns of the specimen surface of (a) SBT, (b) SBT1, (c) SBT2, and (d) SBT4 sintered at 1150°C.

detected in all specimens at 1100°C. At 1150°C $SrTa_2O_6$ is found in the specimens of pure $SrBi_2Ta_2O_9$, SBT1, and SBT2 (shown in Fig. 6). However, SBT4 still preserves its original $SrBi_2Ta_2O_9$ structure. XRD patterns also indicate that the intensities of the (*00l*) diffraction peaks such as (006) and (008) peaks for the Bi_2O_3-added specimens are higher than those for pure $SrBi_2Ta_2O_9$. This implies that the grains of the doped specimens exhibit preferred *c*-axis orientation. The phenomena of preferred orientation will be discussed in Section 3.3.

For quantifying the decomposition, the following equation is used:

$$\text{Decomposition ratio (\%)} = 1 - \Sigma I_{SBT(hkl)} / \Sigma (I_{SBT(hkl)} + I_{ST(hkl)}) \quad (2)$$

where $I_{SBT(hkl)}$ and $I_{ST(hkl)}$ are the intensities of the diffraction peaks of $SrBi_2Ta_2O_9$ and $SrTa_2O_6$, respectively, appearing from $2\theta = 20°$ to 45°. The effects of Bi_2O_3 addition and sintering temperature on the decomposition of $SrBi_2Ta_2O_9$ are presented in Fig. 7. No decomposition of $SrBi_2Ta_2O_9$ occurs in all specimens after sintering up to 1100°C. However, sintering at 1150°C, the decomposition ratios of SBT, SBT1, and SBT2 are found to be 23·9, 11·4, and 11·2%, respectively. SBT4 also starts to decompose when the temperature increases to 1200°C.

In order to realize the decomposition ratio of $SrBi_2Ta_2O_9$ for the bulk of specimens, not only the specimen surface, the sintered specimens were ground to powder and analyzed by XRD (shown in Fig. 8). No detectable traces of $SrTa_2O_6$ could be observed in all ground specimens after 1150°C-sintering. The results for the bulk of specimens have a similar trend as those for the specimen surface. Comparison of Fig. 7 with Fig. 8 reveals that the decomposition ratio on the specimen surface is much greater than that in the bulk of specimens. This result implies that the volatility of Bi_2O_3 from the surface plays an important role in the decomposition process. One typical microstructure for the decomposed specimens is presented in Fig. 9. This figure shows the SEM fractograph of 1250°C-sintered SBT4. It is observed that a porous region is formed near the surface of the specimen, and a dense region is formed beneath the porous region. This is supported by EDS analysis which confirmed that the porous region is $SrTa_2O_6$, and the dense region is $SrBi_2Ta_2O_9$. These results lead to conclusion that the decomposition reaction of $SrBi_2Ta_2O_9$ occurs from the surface of the specimen, and the decomposition zone gradually moves into the bulk.

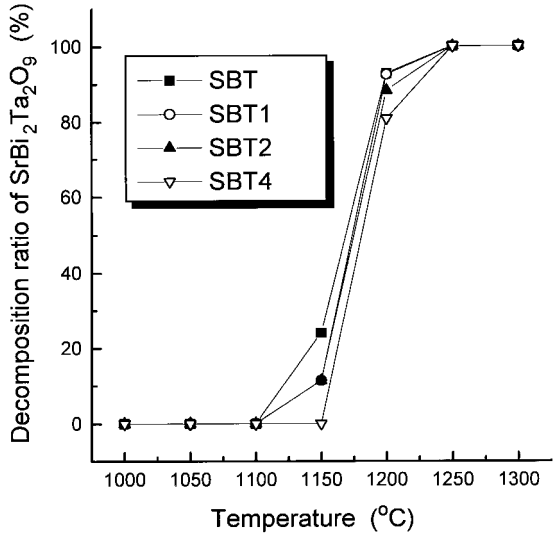

Fig. 7. Decomposition ratio of $SrBi_2Ta_2O_9$ on the specimen surface as a function of sintering temperature.

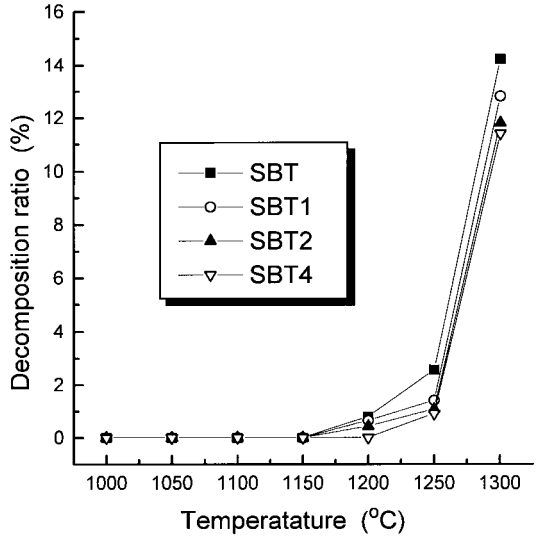

Fig. 8. Decomposition ratio of $SrBi_2Ta_2O_9$ in the bulk of specimens as a function of sintering temperature.

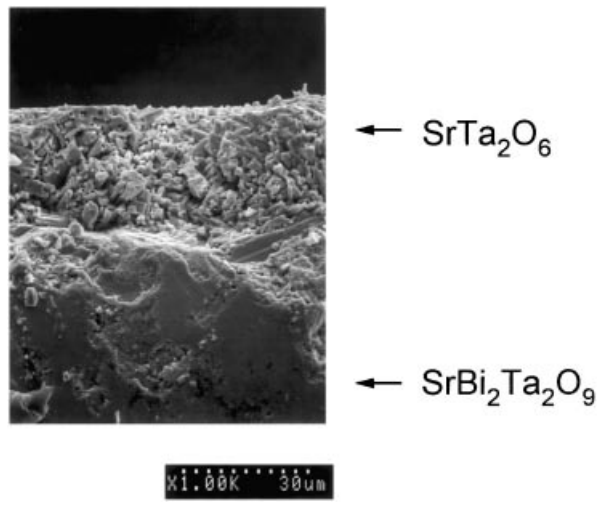

Fig. 9. SEM fractograph of SBT4 sintered at 1250°C for 1 h.

3.3 Effects of the addition of excess Bi_2O_3 on the preferred orientation and microstructure of $SrBi_2Ta_2O_9$

As shown in Figs 5 and 6, the (*00l*) diffraction peaks on the surface of the Bi_2O_3-doped specimens have higher diffraction intensity than those of pure $SrBi_2Ta_2O_9$, showing a *c*-axis preferred orientation. The degree of *c*-axis preferred orientation (*F*) is given by:[32]

$$F = (P - P_0)/(1 - P_0) \tag{3}$$

where $P = \dfrac{\Sigma I_{SBT(00l)}}{\Sigma I_{SBT(hkl)}}$, and $\Sigma I_{SBT(00l)}$ and $\Sigma I_{SBT(hkl)}$ are the sum of intensities of the (*00l*) reflections and that of the (*hkl*) reflections in the sintered specimens, respectively; P_0 is the value of *P* for random orientated powder. Thus, the value of *F* is equal to zero for random orientation and one for complete *c*-axis orientation. Figure 10 shows the *F* factor for specimens sintered at 1050, 1100, and 1150°C as a function of added Bi_2O_3. For pure $SrBi_2Ta_2O_9$ and SBT1, no obvious preferred *c*-axis orientation is observed. With more Bi_2O_3 addition (for SBT2 and SBT4), the specimens exhibit progressing stronger *c*-axis orientation. Furthermore, raising the sintering temperature also significantly enhances the degree of *c*-axis orientation.

In order to understand the origin of the *c*-axis preferred orientation, the microstructures of the specimen surfaces were examined. When no excess

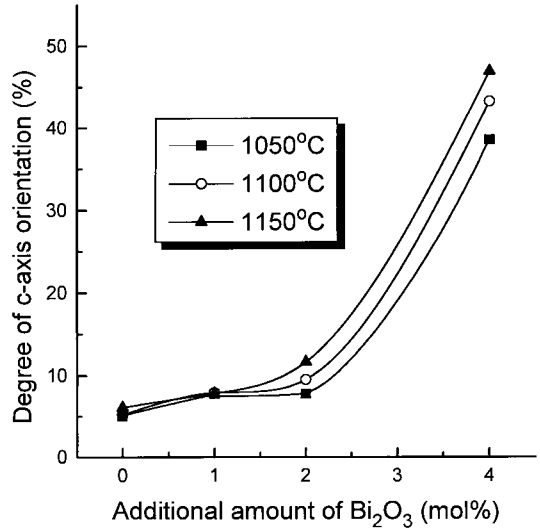

Fig. 10. Degree of *c*-axis orientation for specimens sintered at 1050, 1100 and 1150°C for 1 h.

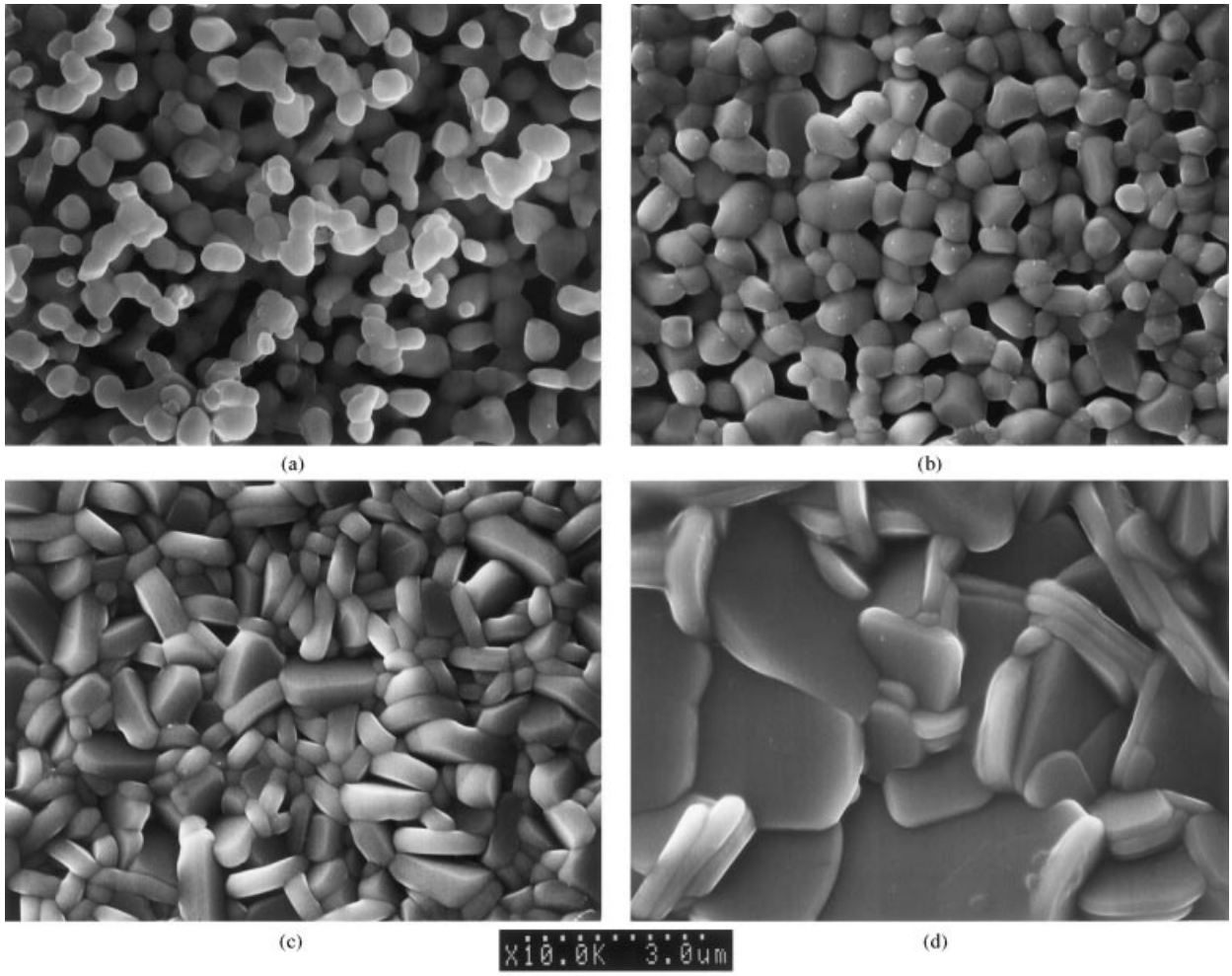

Fig. 11. SEM photographs of (a) SBT, (b) SBT1, (c) SBT2, and (d) SBT4 sintered at 1100°C for 1 h.

Bi_2O_3 is added, a porous microstructure is observed [shown in Fig. 11(a)], confirming the low sinterability of undoped $SrBi_2Ta_2O_9$. The grain size of this specimen is found to be slightly coarsened to 0·5–1 μm. With 1 mol% added Bi_2O_3 (SBT1), large amounts of pores still exist as shown in Fig. 11(b). In these two specimens, the morphology of the grains remains nearly equal-axial. With more Bi_2O_3, specimens reveal higher density [SBT2 in Fig. 11(c)], and the morphology of grains becomes elongated with an aspect ratio around 2–3 and a size of 0·8–1·5 μm. The morphology of SBT4 grains [Fig. 10(d)] is plate-like with a high aspect ratio of around 5–6 (0·5–1 μm in thickness and 3–5 μm in length).

It has been reported that the grains of layered-perovskite materials are inclined to grow along a-b planes and to develop a plate-like morphology in the presence of molten-salts or liquid phases at elevated temperatures.[33,34] When Bi_2O_3 is added in $SrBi_2Ta_2O_9$, the resulting liquid phase enhances anisotropic grain growth. It also appears that in the liquid phase the basal a-b planes of grains develop parallel toward the pressed specimen surfaces. As a consequence, the addition of Bi_2O_3 to $SrBi_2Ta_2O_9$ not only significantly improves the sinterability, but also markedly enhances the preferred orientation at the surface of sintered specimens.

4 Conclusions

The sintering and decomposition of $SrBi_2Ta_2O_9$ have been investigated. Sintering at low temperatures ($\leq$1150°C) is ineffective. Raising the temperature to above 1200°C increases the density of specimens, but also leads to formation of the porous secondary phase-$SrTa_2O_6$. When Bi_2O_3 ($\geq$2 mol%) is added to $SrBi_2Ta_2O_9$, the sinterability is substantially improved. Dense and stable $SrBi_2Ta_2O_9$ ceramics are successfully achieved. The Bi_2O_3 addition also influences the microstructure, and increases both the degree of *c*-axis preferred orientation and the grain size.

Acknowledgements

The authors would like to thank the National Science Council, Taiwan, the Republic of China, for financial support of this study under Contract No. NSC 86-2815-C002-017.

References

1. Paz de Araujo, C. A., Cuchiaro, J. D., McMillan, L. D., Scott, M. C. and Scott, F., Fatigue-free ferroelectric capacitors with platinum electrodes. *Nature*, 1995, **374**, 627–629.
2. Jones, R. E. Jr., Maniar, P. D., Moazzami, R., Zurcher, P., Witowski, J. Z., Lii, Y. T., Chu, P. and Gillespie, S. J., Ferroelectric non-volatile memories for low-voltage, low-powder applications. *Thin Solid Films*, 1995, **270**(1-2), 584–588.
3. Jones, R. E. Jr. and Desu, S. B., Process integration for nonvolatile ferroelectric memory fabrication. *Mater. Res. Soc. Bull.*, 1996, **21**(6), 55–58.
4. Al-Shareef, H. N., Kingon, A. I., Chen, X., Bellur, K. R. and Auciello, O., Contribution of electrodes and microstructures to the electrical properties of $Pb(Zr_{0.53}Ti_{0.47})O_3$ thin film capacitors. *J. Mater. Res.*, 1994, **9**(11), 2968–2975.
5. Kushida-Abdelghafar, K., Miki, H., Yano, F. and Fujisaki, Y., $IrO_2/Pb(Zr_xTi_{1-x})O_3$(PZT)/Pt ferroelectric thin-film capacitors resistant to hydrogen-annealing damage. *Jpn. J. Appl. Phys.*, 1997, **36**(8A), 1032–1034.
6. Yoshimori, H., Watanabe, H., Paz de Araujo, C. A., McMillan, L. D., Cuchiaro, J. D. and Scott, M. C., US Patent No. 9310021, 1993.
7. Aurivillius, B., Mixed bismuth oxides with layer lattices I. The structure type of $CaNb_2Bi_2O_9$. *Arkiv for Kemi*, 1949, **1**(48), 463–480.
8. Subbarao, E. C., A family of ferroelectric bismuth compounds. *J. Phys. Chem. Solids*, 1962, **23**, 665–676.
9. Rae, A. D., Thompson, J. G. and Withers, R. L., Structure refinement of commensurately modulated bismuth strontium tantalate, $Bi_2SrTa_2O_9$. *Acta Cryst. B*, 1992, **48**(4), 418–428.
10. Park, S. S., Yang, C. H., Yoon, S. G., Ahn, J. H. and Kim, H. G., Characterization of ferroelectric $SrBi_2Ta_2O_9$ thin films deposited by a radio frequency magnetron sputtering technique. *J. Electrochem. Soc.*, 1997, **144**(8), 2855–2858.
11. Song, T. K., Lee, J.-K. and Jung, H. J., Structural and ferroelectric properties of the *c*-axis oriented SBT thin films deposited by the radio-frequency magnetron sputtering. *Appl. Phys. Lett.*, 1996, **69**(25), 3839–3841.
12. Lee, J. K., Jung, H. J., Aucielto, O. and Kingon, A. I., Electrical characterization of $Pt/SrBi_2Ta_2O_9/Pt$ capacitors fabrication by the pulsed laser ablated deposition technique. *J. Vac. Sci. Technol. A*, 1996, **14**(3), 900–904.
13. Yang, H. M., Luo, J. S. and Lin, W. T., In situ growth of fatigue free $SrBi_2Ta_2O_9$ films by pulsed laser ablation. *J. Mater. Res.*, 1997, **12**(4), 1145–1151.
14. Desu, S. B., Vijay, D. P., Zhang, X. and He, B. P., Orientation growth of $SrBi_2Ta_2O_9$ ferroelectric thin films. *Appl. Phys. Lett.*, 1996, **69**(12), 1719–1721.
15. Tsai, H. M., Lin, P. and Tseng, T. Y., $Sr_{0.8}Bi_{2.5}Ta_{1.2}Nb_{0.9}O_{9+x}$ ferroelectric thin films prepared by two-target off-axis radio frequency magnetron sputtering. *Appl. Phys. Lett.*, 1998, **72**(14), 1787–1789.
16. Amanuma, K., Hase, T. and Miyasaka, Y., Preparation and ferroelectric properties of $SrBi_2Ta_2O_9$ thin films. *Appl. Phys. Lett.*, 1995, **66**(2), 221–223.
17. Chu, P. Y., Jones, R. E. Jr., Zurcher, P., Taylor, D. J., Jiang, B., Gillespie, S. L. and Lii, Y. T., Characteristics of spin-on ferroelectric $SrBi_2Ta_2O_9$ thin film capacitors for FERAM applications. *J. Mater. Res.*, 1996, **11**(5), 1065–1069.
18. Lu, C. H. and Fang, B. K., Secondary-phase formation and microstructural development in the interaction between $SrBi_2Ta_2O_9$ films and $Pt/Ti/SiO_2/Si$ substrates. *J. Mater. Res.*, 1997, **12**(8), 2104–2110.
19. Li, T., Zhu, Y., Desu, S. B., Peng, C. H. and Nagata, M., Metalorganic chemical vapor deposition of ferroelectric $SrBi_2Ta_2O_9$ thin films. *Appl. Phys. Lett.*, 1996, **68**(5), 616–619.
20. Boyle, T. J., Buchheit, C. D., Rodriguez, M. A., Al-Shareef, H. N., Hernandez, B. A., Scott, B. and Ziller, J. W., Formation of SBT: part I, synthesis and characterization of a novel "sol-gel" solution for production of

ferroelectric $SrBi_2Ta_2O_9$ thin films. *J. Mater. Res.*, 1996, **11**(9), 2274–2281.
21. Kato, K., Zheng, C., Finder, J. M., Dey, S. K. and Torii, K., Sol-gel route to ferroelectric layer-structured perovskite $SrBi_2Ta_2O_9$ and $SrBi_2Nb_2O_9$ thin films. *J. Am. Ceram. Soc.*, 1998, **81**(7), 1869–1875.
22. Al-Shareef, H. N., Dimos, D., Boyle, T. J., Warren, W. L. and Tuttle, B. A., Qualitative model for the fatigue free behavior of $SrBi_2Ta_2O_9$. *Appl. Phys. Lett.*, 1996, **68**(5), 690–692.
23. Chen, T. C., Thio, C. L. and Desu, S. B., Impedance spectroscopy of $SrBi_2Ta_2O_9$ and $SrBi_2Nb_2O_9$ ceramics correlation with fatigue behavior. *J. Mater. Res.*, 1997, **12**(10), 2628–2637.
24. Descamps, M., Remiens, D., Chabal, L., Jaber, B. and Thierry, B., New generation of oxide target for the deposition of ferroelectric thin films by sputtering. *Appl. Phys. Lett.*, 1995, **66**(6), 685–687.
25. Bhattacharya, D., Singh, R. K. and Holloway, P. H., Laser-target interactions during pulsed laser deposition of superconductung thin films. *J. Appl. Phys.*, 1991, **70**(10), 5433–5439.
26. Lu, C. H. and Lee, J. T., Strontium bismuth tantalate layered ferroelectric ceramics: reaction kinetics and thermal stability. *Ceram. Inter.*, 1998, **24**(4), 285–291.
27. Lu, C. H. and Fang, B. K., Solid-state reactions and sintering behavior of layered-perovskite ceramics: barium bismuth tantalate. *J. Mater. Res.*, 1998, **13**(8), 2262–2268.
28. Galasso, F., Katz, L. and Ward, R., Tantalum analogs of the tetragonal tungsten bronzes. *J. Am. Chem. Soc.*, 1959, **81**(22), 5898–5899.
29. Bailar, J. C., Emeleus, H. J., Nyholm. S. R. and Trotman-Dickenson, A. F., *Comprehensive Inorganic Chemistry*, Pergamon Press Ltd. Oxford. 1973. p. 602.
30. Villegas, M., Moure, C., Fernandez, J. F. and Duran, P., Preparation and sintering behaviour of submicronic $Bi_4Ti_3O_{12}$ powders. *J. Mater. Sci.*, 1996, **31**(4), 949–955.
31. Peigney, A. and Rousset, A., Phase transformations and melting effects during the sintering of bismuth-doped zinc oxide powders. *J. Am. Ceram. Soc.*, 1996, **79**(8), 2113–2126.
32. Lotgering, F. K., Topotactical reactions with ferrimagnetic oxides having hexagonal crystals structures — I. *J. Inorg. Nucl. Chem.*, 1959, **9**(2), 113–123.
33. Lin, S. H., Swaetz, S. L., Schulze, W. A. and Biggers, J. V., Fabrication of grain-oriented $PbBi_2Nb_2O_9$. *J. Am. Ceram. Soc.*, 1983, **66**(12), 881–884.
34. Watanabe, H., Kimura, T. and Yamaguchi, T., Sintering of platelike bismuth titanate powder compacts with preferred orientation. *J. Am. Ceram. Soc.*, 1991, **74**(1), 139–147.